Conversion of Hazardous Diesel Soot Particles into a Novel Highly Efficient 3D Hydrogel for Solar Desalination and Wastewater Purification

Higgins M. Wilson, Shakeelur Raheman A. R, Hyeong Woo Lim, and Sang Joon Lee*

Read Online

ACCESS | Metrics & More | Article Recommendations | SI Supporting Information

ABSTRACT: Diesel particulate matter (DPM) generated as vehicular exhaust is one of the main sources of atmospheric soot. These soot particles have been known to cause adverse health problems in humans and cause acute environmental problems. Despite great efforts for minimizing soot production, research on the disposal and recycling of inevitable diesel soot is scarce. However, DPM consists mainly of carbonaceous soot (DS) that can be easily utilized as a photothermal material for solar desalination. Recently, interfacial solar steam generation using three-dimensional (3D) structures has gained extensive attention. 3D-structured hydrogels have exhibited incredible performance in solar desalination owing to their tunable physicochemical properties, hydrophilicity, intrinsic heat localization, and excellent water transport capability. Herein, a novel DS-incorporated 3D polyvinyl alcohol (PVA)-based hydrogel is proposed for highly efficient solar desalination. The polymer network incorporated with purified DS (DS_H) achieved an excellent evaporation rate of 3.01 kg m^{-2} h^{-1} under 1 sun illumination due to its vertically aligned water channels, hydrophilicity, and intrinsic porous structure. In addition, the DS_H-PVA hydrogel could generate desalinated water efficiently (2.5 kg m^{-2} h^{-1}) with anti-salt fouling properties. The present results would motivate the utilization and recycling of waste materials like DS as photothermal materials for efficient, low-cost, and sustainable solar desalination.
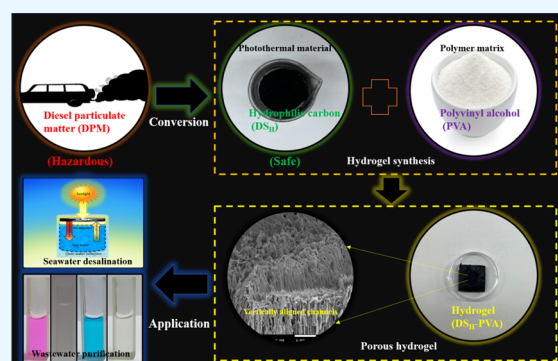
1. INTRODUCTION

Fresh water scarcity has become one of the major global issues seeking urgent and sustainable solutions owing to the rapidly increasing demand for fresh water with population explosion, industrialization, and contamination of limited natural resources.[1,2] Despite extensive studies on sustainable water purification technologies, there is still a great demand for innovative and green water purification techniques due to the requirement of external energy supply and large-scale infrastructure in conventional water purification technologies.[3] Solar-driven desalination has recently gained large attention in this regard with the recent introduction of interfacial solar−thermal steam generation (ISSG) technique which focuses on the evaporation of water molecules at the air−water interface rather than the boiling of bulk water solution.[4−6] ISSG-based desalination has emerged as a promising sustainable and green solution to fresh water shortage problem owing to its superior photothermal efficiency, facile infrastructure, and cost effectiveness.[7] However, this technique is in its nascent stage of development and requires further detailed studies on efficient photothermal materials, micro-/nanostructures, and configuration designs for its applicability in large-scale systems.[8]

Numerous solar steam generators with extremely high evaporation rates and near 100% SSG efficiencies have been introduced recently.[9] In each case, the photothermal materials play a crucial role with its high solar absorption capability of >95% in solar spectra and convert the incoming solar energy into heat at the air−water interface.[10,11] For example, metallic nanoparticles like Au, carbon-based materials like graphene, semiconductor materials like MoS_2 and polymeric materials such as polypyrrole have been utilized extensively.[9,11,12] Among them, carbon-based materials have gained large attention owing to their black body features like light absorption, low-cost, and facile fabrication procedure.[13] However, few reports focused on the use of waste materials like soot as photothermal materials.[4,14,15] In addition, reports on the utilization of diesel soot (DS) particles extracted from heavy vehicles for ISSG are negligible. In our previous report, we discussed an innovative idea of the usage of hydrophobic
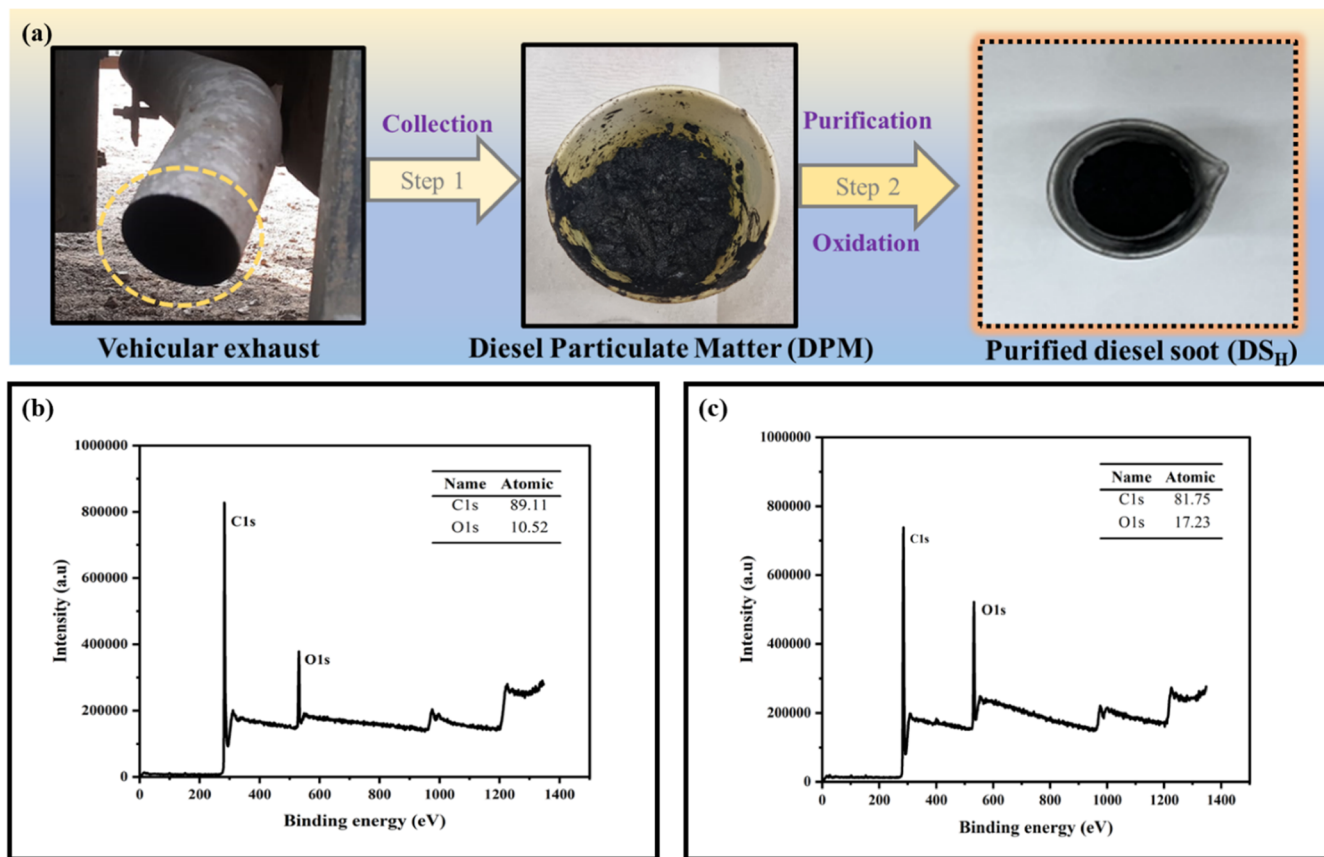
Figure 1. (a) Schematic diagram showcasing the conversion of toxic DPM into DS_H. XPS survey scan spectra of (b) DPM and (c) DS_H.

diesel soot particles extracted by acid treatment of vehicular exhaust as a photothermal material for two-dimensional (2D) interfacial solar—thermal steam generators.[16] However, there was no further reports on photothermal diesel soot-based solar steam generators as far as we surveyed. DS is the primary composition of diesel particulate matter (DPM) that are mainly emitted by diesel engines.[17] DS particles, unlike other soot particles such as candle soot, are a major health hazard owing to the increasing toxic emissions from diesel engines.[18] They have been known to cause acute health issues in humans and animals due to their sub-micrometer size and adverse environmental influence as one of the major causes of air pollution.[19−21] Hence, there has been several efforts to reduce the production of DPM. However, since soot particles are inevitably produced, there is a strong demand to recycle them effectively in different applications.

Heat localization and water transportation also play a significant role in ISSG performance.[22,23] Recently, the 3D structure of photothermal solar absorber have gained large traction in this regard owing to their intricate design that enhance heat localization at the air—water interface.[24,25] In addition, the modifications in water channels and environmental heating due to increased side surface area have led to the superior SSG performance in 3D hydrogels compared to 2D ones.[26−30] 3D structures like hydrogels are the recent evolution in ISSG-based solar desalination.[31−34] The 3D hydrogel composed of crosslinked polymer networks have several advantages in ISSG owing to their tunable physicochemical properties.[35,36] The presence of hydrophilic functional groups attached to the polymeric networks makes it extremely hydrophilic and water absorbent. Polyvinyl alcohol

(PVA) is a common polymer utilized for ISSG because of its high hydrophilicity, non-toxicity, low cost, and facile fabrication.[37−39] The water activation state in PVA hydrogels can also be easily tuned by altering the polymer composition and crosslinkers.[40,41] Thus, PVA hydrogels are one of the ideal materials for ISSG.

The graphitic nanoshell-like morphology and black body-like light absorption properties of DS inspire their integration as a photothermal material.[42] However, since DPM consist of various impurities like toxic heavy metals, they need to be purified, and their safety should be verified before application. In this work, hydrophilic DS (DS_H) purified from hazardous DPM vehicular exhaust was fabricated, and it was successfully incorporated into novel PVA hydrogels (DS_H-PVA) for 3D interfacial solar—thermal steam generators. For this, DPM was first thoroughly purified, and the morphology and composition of DS were examined for safety in detail. After verification of the removal of toxic metals and other impurities, DS_H was incorporated into the PVA matrix at different ratios to obtain DS_H-PVA-x (x—concentration of DS_H). After the optimization of DS_H-PVA-x hydrogels, the DS_H-PVA-5 interfacial solar—thermal steam generator could achieve a superior evaporation rate of 3.01 kg m^{-2} h^{-1} at 1 sun irradiation. DS_H-PVA-x was further studied for their heat localization properties and optimized for their application in seawater desalination and water purification. The desalination results were found to be successful under low solar irradiation and DS_H-PVA-5 also exhibited intrinsic salt rejection capability. This work should promote the utilization and recycling of waste products for highly efficient seawater desalination and wastewater treatment.
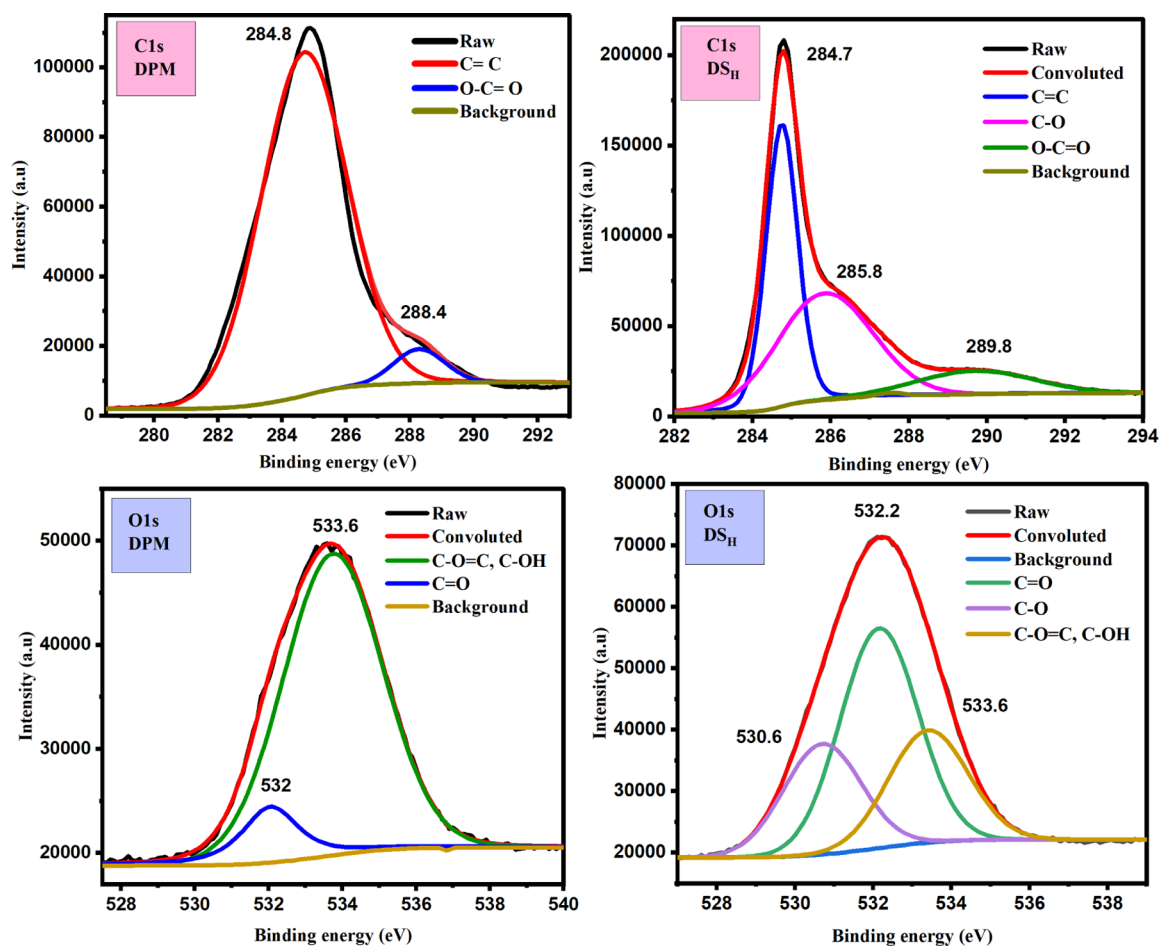
Figure 2. C 1s and O 1s spectra of DPM and DS$_H$.

2. EXPERIMENTAL SECTION

2.1. Materials. DPM was collected from the exhaust pipes of diesel-powered cars at a local garage in Pohang, South Korea. PVA (M_n = 15 000−23 000 g mol^{-1}), potassium permanganate (KMnO$_4$), and hydrogen peroxide (H$_2$O$_2$, AR grade) were purchased from Sigma-Aldrich. All materials and reagents were used without any purification.

2.2. Purification of DPM and Fabrication of DS$_H$. The collected DPM was purified as illustrated in Figure 1. DPM was first washed with ethanol (95% purity) and hexane several times to remove the unused petroleum products. The washed DPM was then dried at room temperature for further experimentation. DS$_H$ was fabricated by modifying a previous report.[17] 1 g of DPM was stirred with 50 mL of conc. H$_2$SO$_4$ until the reaction mixture was completely mixed. The reaction mixture was stirred for 2 h, and this was followed by the addition of 1 g of KMnO$_4$. It was continuously stirred using a magnetic stirrer for 6 h at 70 °C. A 500 mL solution containing 5 mL of H$_2$O$_2$ in ice-chilled deionized (DI) water was later added to prevent MnO$_2$ precipitation. The obtained solution was filtered using vacuum filtration, its pH was adjusted to neutral, and then dried. The obtained dried solid was named hydrophilic DS (DS$_H$).

2.3. Synthesis of DS$_H$-PVA-x hydrogels. DS$_H$-PVA-x hydrogels were synthesized following a previous literature method with modifications.[43] (Figure 3) At first, an aqueous solution of PVA was made by dissolving 15 g of PVA in 100 mL DI water. The final solution was obtained by heating and

stirring the solution for 2 h at 90 °C until the solution turned transparent and PVA was completely dissolved. To 20 mL of the PVA dissolved solution, 250 μL of 50% glutaraldehyde solution in water was added and stirred for 15 min (solution 1). 500 μL of HCl was later added to this solution and stirred rapidly for 1−2 min using a magnetic stirrer. The solution was rapidly poured into prepared silicon molds (2 × 2 × 2 cm) at room temperature. The solution was then immediately frozen at −20 °C overnight and thawed slowly at room temperature. The obtained hydrogel was named DS$_H$-PVA-0. For incorporation of DS$_H$, three different concentrations of DS$_H$, that is, 2.5, 5, and 10 mg/mL were added into solution 1 before the addition of HCl. The DS$_H$ solutions were first prepared by mixing DS$_H$ in DI water and sonicated for 2 h until the DS$_H$ was dissolved in the solution. After the addition of DS$_H$ solutions, the mixtures were stirred for 10 min using a magnetic stirrer to obtain a uniform dispersion. Finally, 500 μL of HCl was added, stirred, and transferred into silicone molds. Other steps were similar to the fabrication of DS$_H$-PVA-0, and the obtained hydrogels were named DS$_H$-PVA-2.5, DS$_H$-PVA-5, and DS$_H$-PVA-10, respectively.

3. RESULTS AND DISCUSSION

3.1. Fabrication of DS$_H$ and Its Characterization. In ISSG, the broadband light absorbance of photothermal materials capable of is crucial. DS particles have not been utilized adequately although they have black-body-like properties. DPM has been known as a hazardous material because it is
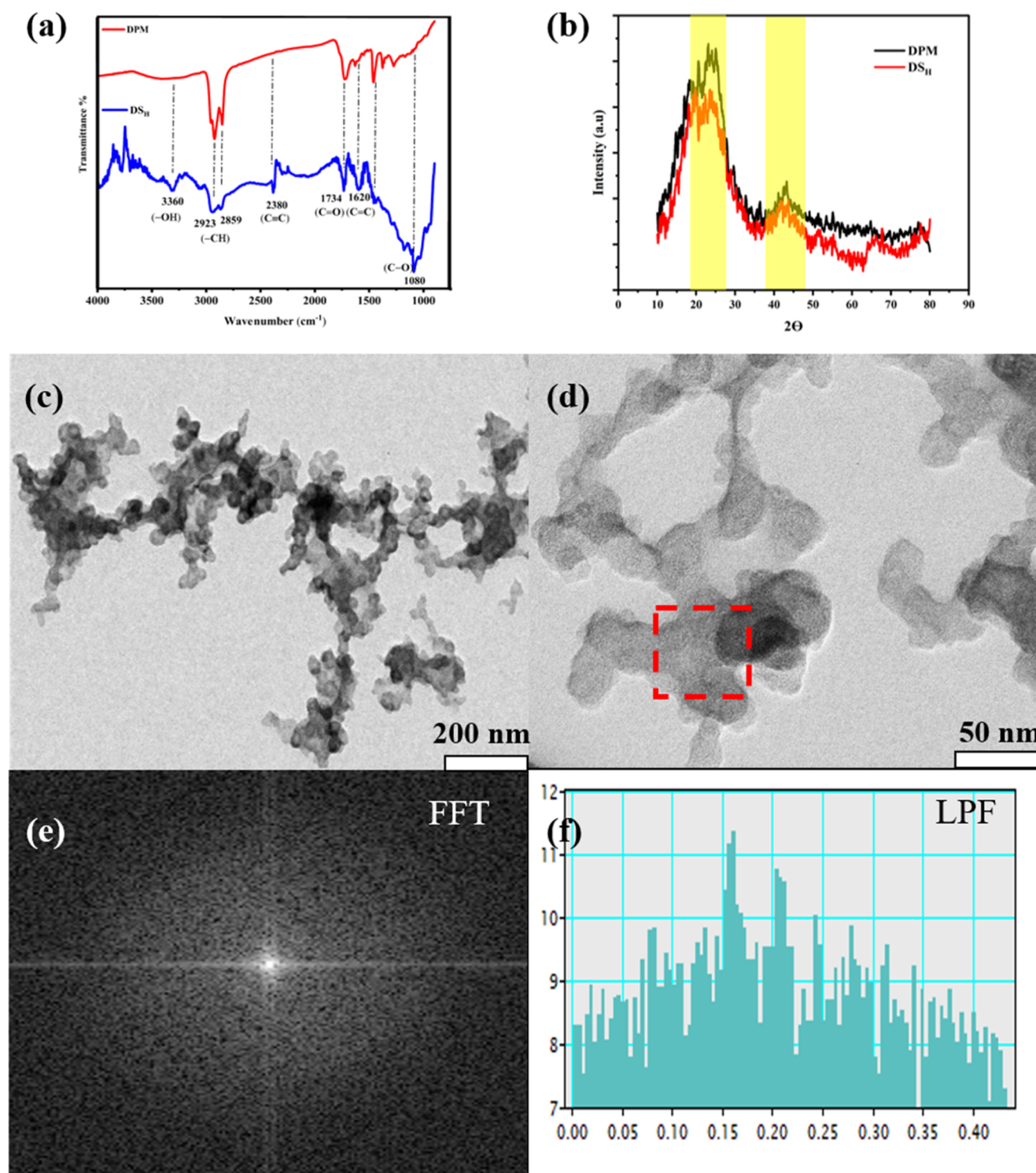
Figure 3. (a) FTIR and (b) XRD spectra of DPM and DS_H. (c,d) TEM images of DS_H. (e,f) FFT diffractogram and line profile of DS_H, respectively.

generated mainly through incomplete combustion of diesel oil. DPM production is increased with deteriorating engine performance. In addition, despite numerous scientific advancements, the production of DPM is inevitable and thus development of novel recycling techniques is strongly required. The composition of DPM varies largely based on the origin of extracted vehicles and it contains toxic heavy metals or other harmful chemical components. However, since carbonaceous

graphitic nanoshell-like particles are a major constituent, they can be utilized effectively in energy-related applications.[17] Figure 1a shows the purification and conversion process of DPM into hydrophilic DS_H. The collected DPM was first washed with organic solvents like hexane and ethanol to remove petroleum components and other organic impurities. In the next step, oxidizing agents like potassium permanganate ($KMnO_4$) was utilized to functionalize the hydrophobic DS
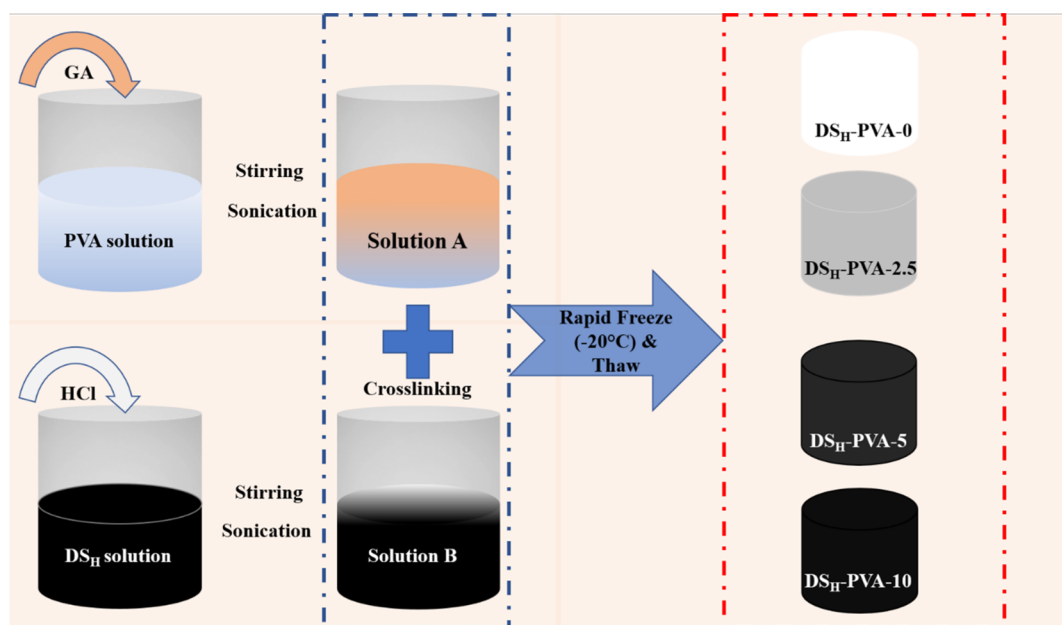
Figure 4. Schematic illustration of the synthesis of DS_H-PVA hydrogels.

particles into DS_H as described in detail in Section 2.2. In the first step, the purification of DPM was verified using energy-dispersive spectroscopy (EDS) analysis (Figures S1 and S2). According to EDS analysis, DPM has approximately 92.25% weight of carbon, 7.37% weight of oxygen, and very small impurities of copper and zinc accounting for 0.2 and 0.7%, respectively. In contrast, DS_H has 77.80% weight of carbon, 21.77% weight of oxygen, and small impurities of copper and zinc of 0.24 and 0.19%, respectively. The increased oxygen weight % in DS_H is attributed to the modification of oxygen-containing groups on the surface. In addition, no toxic heavy metals or other impurities are found. This implies that DS_H is a safe material for further experimentation. X-ray photoelectron spectroscopy (XPS) analysis was carried out to further evaluate the composition of DPM and DS_H (Figures 1b,c and 2). The survey scan results are similar to the EDS analysis. The results indicate ∼6% increase in oxygen content in DS_H, signifying the addition of oxygen functional groups on the soot surface. Figure 2 shows the high-resolution spectra of DPM and DS_H. The C 1s spectra of DPM was deconvoluted into two peaks at 284.8 and 288.4 eV. The peak at 284.4 eV corresponds to the C=C bond. In DS_H C 1s spectra, this C=C peak intensity decreases with an increase in various other oxygen-containing functional groups and the sp^3 carbon group. The high-resolution O 1s spectra of DPM display two major peaks at 532 and 533.6 eV which correspond to the C=O bond and C−O−C and C−OH bonds, respectively.[44,45] In the case of DS_H, the intensity of the 533.6 eV peak decreases, and a new additional peak is observed at 530.6 eV which is attributed to the −COO bonding. This confirms that oxygen-containing functional groups are formed during the synthesis of DS_H.[46]

For further understanding the chemical structures of DPM and DS_H, Fourier transform infrared (FTIR) analysis was conducted, and the results are shown in Figure 3a. The absorption peak at 3360 cm^{-1} is attributed to −OH vibrations associated with hydrogen bonding, phenolic hydroxyl, and N−H stretching vibrations.[47] The −OH peak's strength is significantly increased in DS_H, indicating the increase of oxygen functional groups. This can enhance the hydrophilicity

of DS_H. The DPM and DS_H show bands at 2859 and 2925 cm^{-1}, respectively, which correspond to the stretching vibrations of the −CH group. The band at 1734 cm^{-1} is associated with the (O=C−OH) stretching vibration. After the treatment of DS, two broadened peaks appear at 1620 and 1080 cm^{-1}, which correspond to the new functional groups (C=C) and C−O, respectively. These results confirm that the DPM surface is modified.

To evaluate the degree of crystallinity or amorphous structure of DPM and DS_H, X-ray diffraction (XRD) analysis was performed, as shown in Figure 3b. The high-intensity diffraction peaks at angles 24.1 and 23.3° are assigned to the (002) plane. The spacing of the aromatic layer in graphitic carbon is usually recognized by the peak position at the (002) plane. The presence of a low-intensity diffraction peak at an angle of 43.1° further supports the existence of a graphitic structure. The interplanar distances of DS_H for these peaks at 3.8 Å are increased compared to DPM (3.7 Å). This results from the presence of amorphous carbon and surface defects in DS_H.[48] The morphological structure of DS_H was observed using scanning electron microscopy (SEM), whose images are depicted in Figure S3. The SEM image shows an agglomeration of soot particles. Transmission electron microscopy (TEM) was utilized for further detailed observation of these particles (Figure 3c,d). The TEM images display spherules gathered in large quantities to produce fractal-like geometric structures.[49] The average particle size of treated DS is in the range of 30−50 nm. In Figure 3d, the dotted square represents the position at which the fast Fourier transform (FFT) diffraction pattern was obtained (Figure 3e). The FFT diffractograms demonstrate that the DS_H structure is totally amorphous, with no anisotropy or discernible sp^2-rich clusters. The disorder line profile of the treated DS shown in Figure 3f also confirms the amorphous structure of DS_H.

3.2. Fabrication and Characterization of DS_H-PVA-x Hydrogels. The hydrogels were synthesized by chemical crosslinking and freeze/thawing (physical crosslinking), as shown in Figure 4. This fabrication procedure followed a previous study where both the chemical and physical
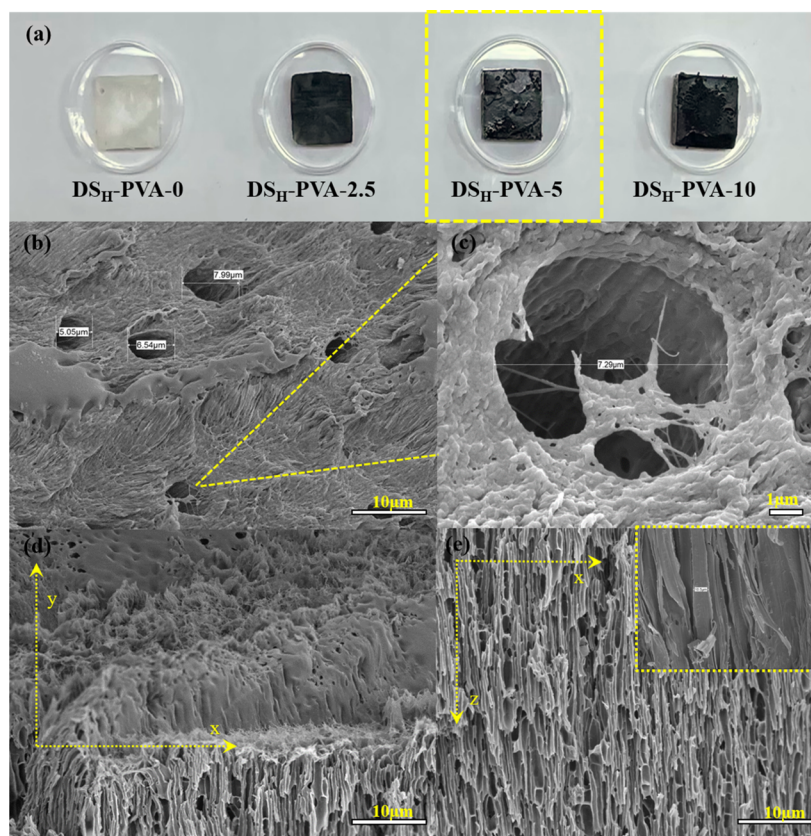
Figure 5. (a) Digital photographs of DS$_H$-PVA-x hydrogels. (b,c) SEM images of the DS$_H$-PVA-5 hydrogel under different magnifications. (d) Cross-sectional SEM image of DS$_H$-PVA-5. (e) Cross-sectional SEM image of DS$_H$-PVA-5 showing vertically aligned channels. The inset shows the magnified image of channels.
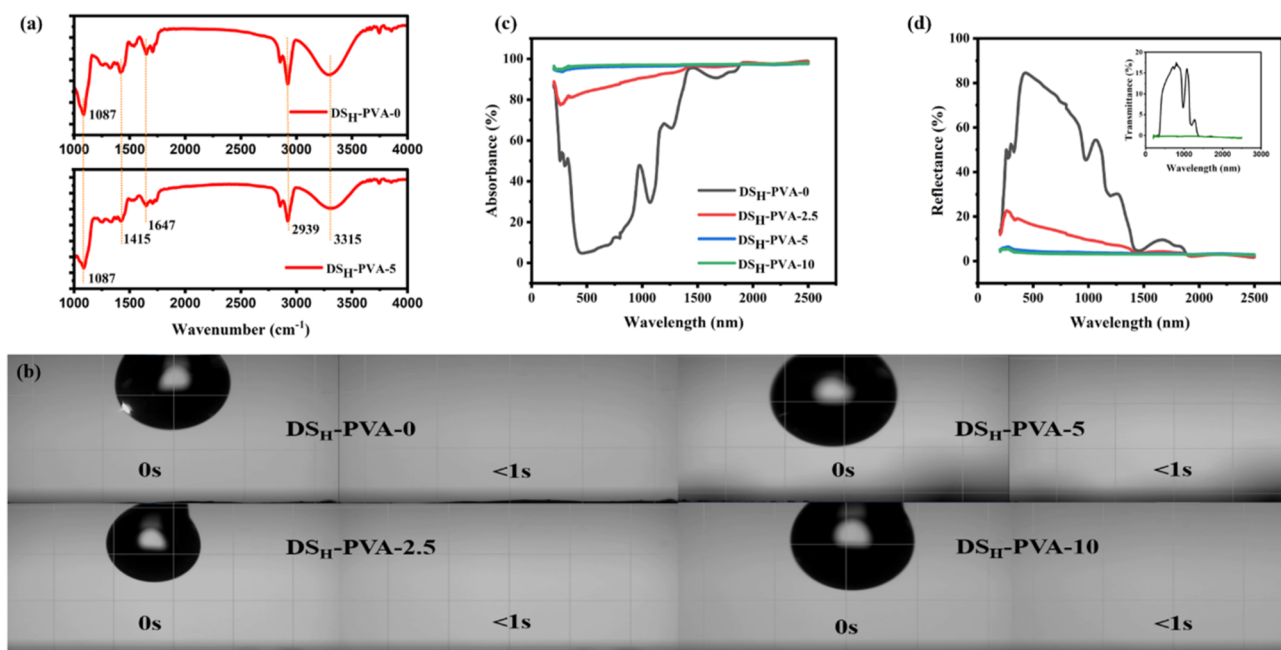

Figure 6. (a) FTIR spectra, (b) CA measurements, (c) absorption spectra, and (d) reflectance and transmittance spectra (inset) of DS$_H$-PVA-x hydrogels.

crosslinking were utilized for improving the mechanical strength and stability of hydrogels in water.[43] After complete purification of DPM and its successful oxidation to DS$_H$, it was incorporated into the PVA polymer matrix at different ratios,

as described in detail in Section 2.3. For comparison, first DS$_H$-PVA-0 (DS$_H$ = 0 mg) was fabricated. Three ratios of DS$_H$ (2.5, 5, and 10) were chosen and successfully incorporated into the PVA polymer matrix (Figures 4 and 5a). The addition of DS$_H$
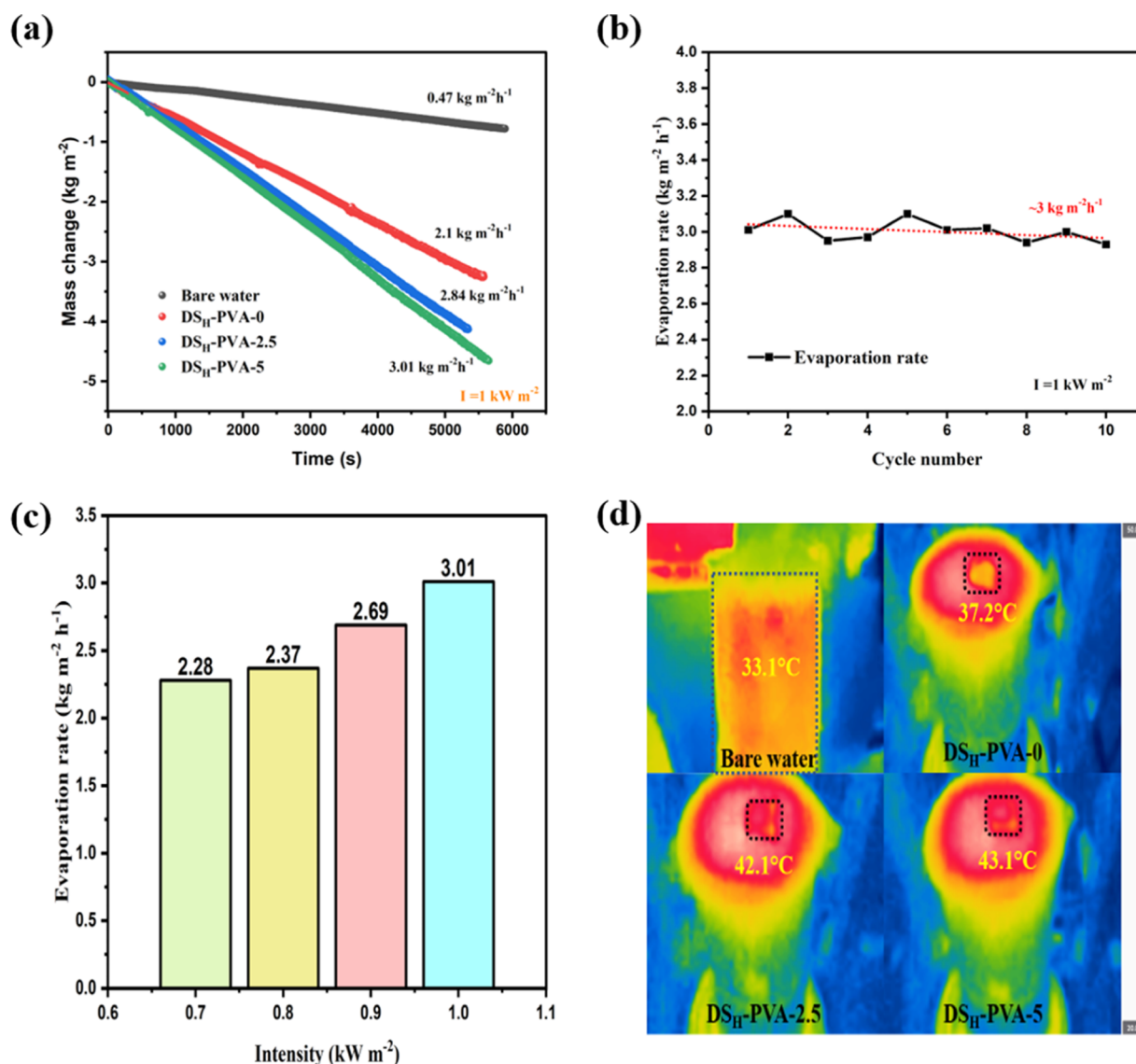
Figure 7. (a) ISSG performance of hydrogels. (b) Cyclic stability performance of the DS$_H$-PVA-5 hydrogel. (c) ISSG performance of the DS$_H$-PVA-5 hydrogel under 0.7−1 sun illumination. (d) IR thermal images of steam generator systems after 60 min of 1 sun illumination.

was observed to change the color of hydrogels to black (Figure 5a). It is worthwhile to note that the oxidation of DS$_H$ plays a crucial role in the uniform suspension of DS$_H$ in water and its later combination with solution A in the formation of gel. For further understanding the deposition and formation of DS$_H$-PVA-x hydrogels, SEM images were captured and are illustrated in Figure 5b,c. The SEM images of the top surface display a flat sheet-like microporous structure having a rough outer surface with small pores ranging from 5 to 8 μm in diameter. The pores are randomly distributed across the top surface. This is attributed to the utilization of both chemical and physical crosslinkers simultaneously in the hydrogel synthesis.

A previous study reported that the temperature and time of freeze thawing played a crucial role in the development of ice crystals during hydrogel fabrication.[43] It was hypothesized that the growth of the ice crystals is delayed with immediate freezing after chemical crosslinking. To further verify this hypothesis, the DS$_H$-PVA-5 hydrogel was fabricated by immediate freezing at −80 °C. The captured SEM images show a flat irregular surface with no porosity (Figure S4). This

suggests that a colder temperature delays the ice-crystal formation in the PVA matrix and affects the pore size and channels in PVA hydrogels. These results confirm that temperature plays a crucial role in freeze thawing after chemical crosslinking of PVA. The slow ice-crystal formation also leads to the development of vertically aligned water channels inside the hydrogel. These vertical channels with an average diameter of 10 μm were observed to be uniformly distributed all across the hydrogel (Figure 5d,e). Hydrogels with small porosity and vertically oriented internal channels are known to have the ability to rapidly transport water from the bottom of the evaporation generator to the top evaporation surface. Furthermore, water can be readily squeezed out of hydrogels under compression condition due to the vertical channels without affecting the general configuration of the hydrogels.

To further examine the composition of hydrogels, EDS and elemental mapping of DS$_H$-PVA-5 hydrogel were conducted, whose results are shown in Figure S5. EDS analysis shows the presence of carbon and oxygen as its main elements with atomic percentages of 78.33 and 21.67%, respectively. The

elemental mapping displays a uniform distribution of carbon and oxygen atoms. In addition, no other elements exist after the incorporation of DS_H into the PVA polymer matrix. FTIR analysis was also utilized to study the chemical composition of hydrogels, which is shown in Figure 6a. The hydrogels display no noticeable differences in their chemical composition. The peaks at 2939,1647, 1087, and 1415 are attributed to C−H stretching vibrations of −CH$_3$, −CH$_2$, C−H ,and C−O groups, respectively.[50,51] The large stretching peak at 3315 cm^{-1} indicates the presence of hydroxyl (O−H) groups that promote hydrophilicity in PVA hydrogels. The addition of DS_H has no influence on the hydrophilic nature of PVA hydrogels. This was further analyzed through contact angle (CA) measurements (Figure 6b). The CA measurements of DS_H-PVA-x hydrogels exhibit superior hydrophilicity in the hydrogels with a CA angle of 0° in each case.

The water transport performance of DS_H-PVA-x hydrogels was also evaluated. In less than 5 s, the dry hydrogel absorbed water rapidly and got completely wet. This indicates that the hydrogels are extremely hydrophilic and can transport water rapidly. The excellent water transport property of hydrogels is mainly attributed to their porosity, vertically aligned channels, and a large number of hydroxyl groups in the PVA polymeric structure. Light absorption is crucial for excellent ISSG performance. In our previous study, we demonstrated the light absorption properties of hydrophobic diesel soot.[16] Similarly, DS_H-PVA-x hydrogels also exhibit light absorption property as shown in Figure 6c,d. DS_H-PVA-0 is white in color and has high reflectance in 250−2500 nm range due to poor light-absorbing capabilities of PVA. The introduction of DS_H dramatically increases the light absorption of DS_H-PVA-5 and DS_H-PVA-10 hydrogels with absorbance values of 96 and 97%, respectively. The broadband light absorption and excellent water transport properties of DS_H-PVA-x hydrogels make them an excellent candidate for long-term ISSG operation.

3.3. ISSG Performance of DS_H-PVA-x Hydrogels. The ISSG performances of fabricated DS_H-PVA-x hydrogels were estimated using a solar simulator, as illustrated in Figure S6. For comparison, the ISSG performance of each hydrogel was evaluated under identical conditions, as described in Section S2. Figure 7a shows the steam generation performance of the hydrogels under 1 sun illumination. At first, the performance of the bare water system without hydrogels or thermal insulation was evaluated as a control. As expected, the control system shows poor ISSG performance (0.47 kg m^{-2} h^{-1}) owing to the poor light absorption of water and high thermal losses induced by bulk heating of water. In the ISSG performance evaluation of hydrogels, each hydrogel was equipped with a polystyrene foam (thermal conductivity = 0.036 W m^{-1} K^{-1}) and airlaid paper setup for thermal insulation and continuous rapid water transport (Figure S7). The addition of thermal insulation to hydrogels shows significant improvement in the ISSG performance. In each case, the mass loss of water varies linearly with time under constant solar illumination. DS_H-PVA-0 which is white in color exhibited the lowest evaporation rate of 2.1 kg m^{-2} h^{-1}. However, the addition of DS_H in hydrogels show substantial enhancement in the ISSG performance. This is largely due to the broadband light absorption capability of DS_H, as described earlier in Section 3.2. The evaporation rate also increases with the increase in concentration of DS_H in DS_H-PVA-x hydrogels. DS_H-PVA-5 shows the highest evaporation rate of 3.01 m^{-2} h^{-1}, followed by DS_H-PVA-2.5 (2.84 kg m^{-2} h^{-1}) which are ~6 times the evaporation rate of the

control bare water system. For optimization, DS_H-PVA-10 was also investigated for its ISSG performance. However, the hydrogel could not sustain its performance after 30 min of constant solar illumination. This might be attributed to the overheating of the hydrogel, leading to the damage of brittle hydrogel structure (Figure S8). Since the characteristics of DS_H-PVA-x hydrogels are similar except for the concentration of DS_H, the ISSG performance variation of each hydrogels results from their light absorption capabilities. The performance evaluation of DS_H-PVA-5 was repeated multiple times to study its long-term durability, and the variation was found to be ~5% after 10 cycles (Figure 7b). This can be attributed to the vertically aligned channels and hydrophilicity of porous DS_H-PVA-5 hydrogels. The excellent ISSG performance of DS_H-PVA-5 is also maintained under lower incident solar intensities (0.7−0.9), as demonstrated in Figure 7c. Hence, DS_H-PVA-5 is a promising candidate for solar desalination under periodically varying daytime natural solar illumination.

The performance of steam generators can be quantified by estimating their photothermal conversion efficiencies, as detailed in Table S1. In each case, the dark evaporation rates were subtracted for accurate evaluations.[4] The steam generation efficiencies of each hydrogels are analogous to their evaporation rates. The excellent steam generation performance of DS_H-PVA-x were further evaluated using IR imaging, as depicted in Figures 7d and S9. The surface temperatures of all hydrogels increase rapidly with the start of solar irradiation and reach a stable equilibrium condition in 2 min (Figure S9). However, the surface temperature varies depending on the DS_H concentration of hydrogels. DS_H-PVA-5 exhibits the highest stable temperature in 60 min (42.1 °C). This is attributed to the increase of DS_H concentration in DS_H-PVA-5. The surface temperature of DS_H hydrogels demonstrates excellent heat localization at the air−water interface. This temperature increase was also confirmed by monitoring the temperature of bulk water separately using a digital thermometer (Figure S10). Based on the results, we can infer that the surface water evaporation is the dominant mechanism in these steam generation systems. For the control bare water system, the surface temperature increases linearly with the lapse of time. This was also further confirmed by the bulk water temperatures measured at the top and bottom section of the vessel (Figure S11). Thus, DS_H-PVA-x hydrogels are excellent in minimizing the conductive heat loss to bulk water and localizing heat efficiently at the air−water interface.

The superior evaporation performance of DS_H-PVA-5 is ascribed to the following factors: 1) DS is an excellent photothermal material and can efficiently convert incoming solar radiation to heat. This translates into excellent light to heat conversion at the air−water interface. b) The hydrophilicity, vertically aligned water channels, and porous structure of DS_H-PVA-x hydrogels ensure quick and continuous transport of water and c) DS_H-PVA-x hydrogels along with the polystyrene foam provide thermal insulation, which corroborates the effective heat localization at the air−water interface.

3.4. Seawater Desalination and Water Purification Performances. The primary application of ISSG devices is solar desalination of seawater. ISSG devices with exceptionally high evaporation rates can provide rapid evaporation of water and generate clean water through evaporation−condensation processes. The seawater desalination performance of the DS_H-PVA-5 hydrogel was investigated using a solar simulator. For
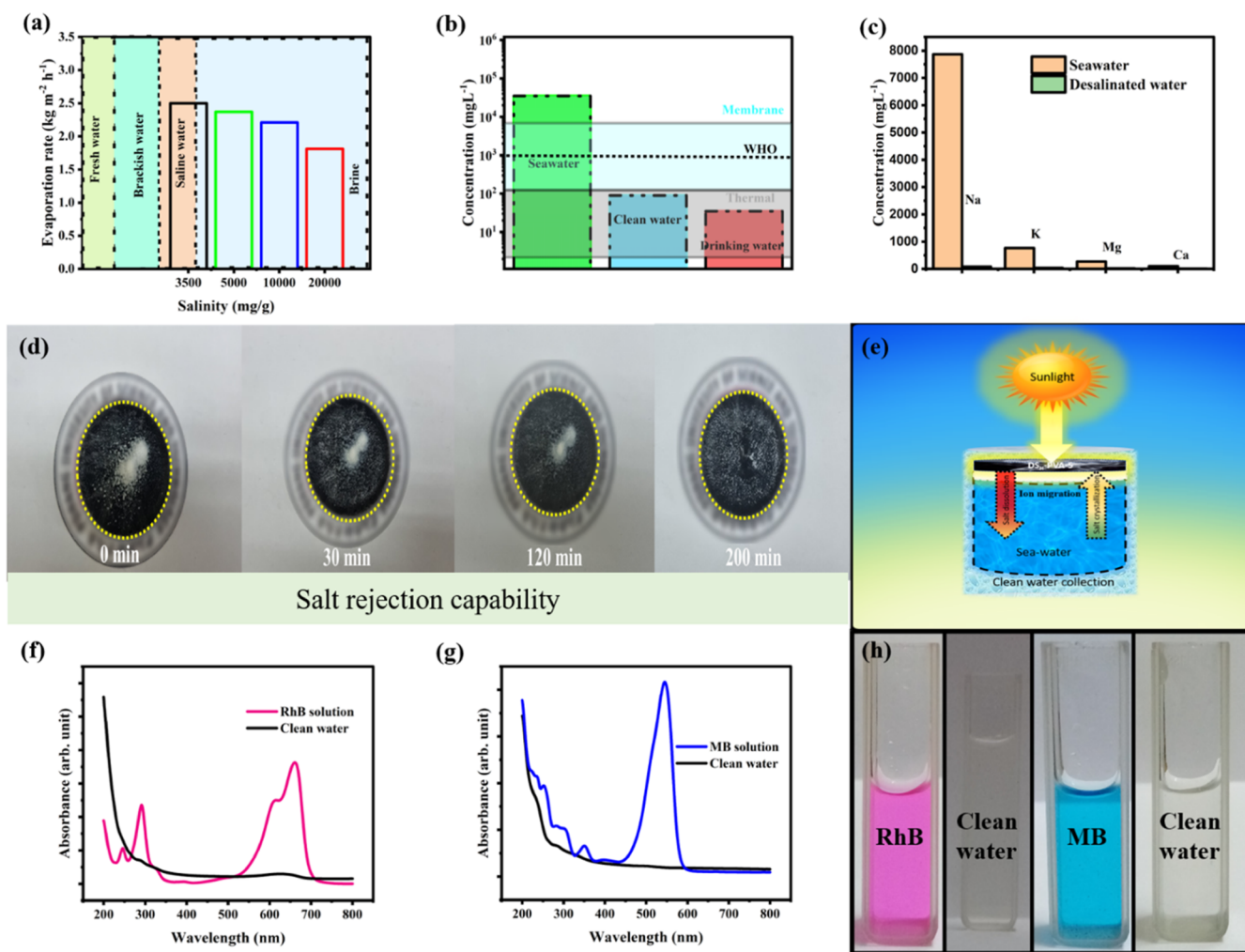
Figure 8. (a) Evaporation rate of DS$_H$-PVA-5 hydrogel at different salinities of seawater under 1 sun illumination. (b) TDS and (c) ICP−OES results after the desalination process. (d) Digital photographs showcasing the salt rejection by the DS$_H$-PVA-5 hydrogel. (e) Schematic illustration of the salt rejection process in the DS$_H$-PVA-5 hydrogel. (f) Absorption spectra of Rhodamine B solution and purified clean water. (g) Absorption spectra of methylene blue solution and purified clean water. (h) Optical images showing the purification of rhodamine B and methylene blue solution.

comparison, the performance of a bare seawater system was also examined under identical conditions. Figure 8a shows the seawater steam generation performance of DS$_H$-PVA-5 under different salinities of seawater. Analogous to pure water, DS$_H$-PVA-5 shows excellent steam generation performance under 1 sun illumination. For 3.5 wt % standard seawater sample, DS$_H$-PVA-5 showed a steam generation rate of 2.5 kg m^{-2} h^{-1} under 1 sun illumination (5 times that of the bare water system). This excellent desalination performance was also maintained for 5, 10 and 20 wt % seawater samples. These results indicate that the DS$_H$-PVA-5 hydrogel is highly efficient in seawater desalination.

The purification ability of DS$_H$-PVA-5 for seawater is shown in Figure 8b. For this purpose, the evaporated water was collected and tested for its salinity through analysis of total dissolved solids (TDS). The collected water was found to have salinity levels at least 4 orders lower than that of raw seawater. The salinity levels are lower than the WHO standard recommended for drinking water. This demonstrates that drinking water can be generated by a facile DS$_H$-PVA-5 hydrogel setup. Inductively coupled plasma optimal emission spectrometry (ICP−OES) was utilized to analyze the quality of

desalinated water. The results showed that the major ions (Na$^+$, Mg^{2+}, K$^+$, and Ca^{2+}) were all significantly reduced by at least 3 orders of magnitude (Figure 8c). These results indicate that DS$_H$-PVA-5 is effective for solar desalination of seawater.

Salt accumulation is another major issue in solar desalination owing to the crystallization of salt crystals at the interface of solar−thermal steam generators.[52] Hence, much focus has been directed toward the fabrication of anti-salt fouling ISSG devices for long-term desalination operation. Hydrogels, owing to their porous structure and intrinsic water channels, have natural salt rejecting capability that prevents the accumulation of salt crystals at the surface. Therefore, the salt rejecting capability of DS$_H$-PVA-5 hydrogels was tested as shown in Figure 8d. For this purpose, salt was deposited on the top surface and monitored continuously using a digital camera. With the start of the experimentation, the salt crystals deposited on top of the hydrogels were quickly dissolved as they came in contact with the hydrogels. In addition, no visible salt accumulation was observed during seawater desalination experiments even for 10 wt % seawater sample. This phenomenon was reported in previous studies where the salt rejecting property was attributed to the ion equilibrium

between water transport-induced ion absorption and diffusion-enabled salt ion discharge.[34] Under constant solar illumination, salt ions are subjected to evaporation-induced transport to the top surface where they tend to crystallize. However, these ions undergo rapid dissolution in the underlying bulk solution under dark conditions owing to the hydrophilicity and vertically aligned water channels of DS_H-PVA-5 hydrogel (Figure 8e).

One of the common contaminants in wastewater is toxic dye particles, such as rhodamine B and methylene blue. The removal of these toxic molecules using evaporation−condensation processes is a facile method for sustainable water purification.[53] To demonstrate this feasibility, two common dye molecules, that is rhodamine B and methylene blue, were chosen as test samples and successfully purified using a PVA-5 hydrogel setup. As expected, the collected purified water samples exhibit no concentration of the corresponding dye contaminants (Figure 8f−h). The purification of such wastewater is attributed to the evaporation−condensation-based water distillation mechanism where water molecules are evaporated, leaving the dye molecules in the bulk solution.

4. CONCLUSIONS

In this study, a highly efficient and low-cost DS_H-PVA-5 hydrogel was made of hydrophilic diesel soot (DS_H) obtained by recycling hazardous DPM as the photothermal material. DS_H was successfully incorporated into the PVA polymer matrix using a combination of chemical (glutaraldehyde) and physical (freeze thawing) crosslinking. The fabricated hydrogels had 3D microporous structures with vertically aligned water channels which promote rapid water transport to the air−water interface. The incorporation of DS_H into PVA significantly improved the light absorption capabilities of DS_H-PVA-x hydrogels. The DS_H-PVA-5 hydrogel achieved a high steam generation rate of 3.01 kg m^{-2} h^{-1} under 1 sun irradiation. In long-term testing, the fabricated hydrogels maintained excellent steam generation performance even under low solar irradiation of 0.7−0.9 sun illumination. The fabricated DS_H-PVA-5 hydrogel also successfully desalinated seawater (3.5 wt %) under 1 sun illumination with an evaporation rate of 2.5 kg m^{-2} h^{-1}. The desalinated water exhibited salinity levels that are comparable to that of traditional drinking water. The hydrogel also exhibited salt rejecting property, demonstrating it as an eligible candidate for long-term seawater desalination. The present results would motivate the utilization of waste materials such as diesel soot as photothermal materials for low-cost, efficient, and sustainable solar desalination applications.

■ ASSOCIATED CONTENT

ⓈⒾ Supporting Information

The Supporting Information is available free of charge at https://pubs.acs.org/doi/10.1021/acsomega.2c07430.

> Additional experimental results, experimental methodology, and photographs of experimental setups (PDF)

■ AUTHOR INFORMATION

Corresponding Author

Sang Joon Lee − *Department of Mechanical Engineering, Pohang University of Science and Technology, Pohang 37673 Gyeongbuk, The Republic of Korea;* ⓞ orcid.org/0000-0003-3286-5941; Email: sjlee@postech.ac.kr

Authors

Higgins M. Wilson − *Department of Mechanical Engineering, Pohang University of Science and Technology, Pohang 37673 Gyeongbuk, The Republic of Korea;* ⓞ orcid.org/0000-0001-6971-8780

Shakeelur Raheman A. R − *Department of Applied Science, Shri Vile Parle Kelavani Mandal's Institute of Technology, Dhule 424001 Maharashtra, India*

Hyeong Woo Lim − *Department of Mechanical Engineering, Pohang University of Science and Technology, Pohang 37673 Gyeongbuk, The Republic of Korea*

Complete contact information is available at:
https://pubs.acs.org/10.1021/acsomega.2c07430

Notes

The authors declare no competing financial interest.

■ REFERENCES

(1) Lewis, N. S. Research Opportunities to Advance Solar Energy Utilization. *Science* **2016**, *351*, aad1920.

(2) Vörösmarty, C. J.; Green, P.; Salisbury, J.; Lammers, R. B. Global Water Resources: Vulnerability from Climate Change and Population Growth. *Science* **2000**, *289*, 284−288.

(3) Selvam, A.; Jain, G.; Chaudhuri, R. G.; Mandal, M. K.; Chakrabarti, S. Avant-Garde Solar-Thermal Nanostructures: Nascent Strategy into Effective Photothermal Desalination. *Sol. RRL* **2022**, *6*, 2200321.

(4) Wilson, H. M.; Rahman A.R, S.; Parab, A. E.; Jha, N. Ultra-Low Cost Cotton Based Solar Evaporation Device for Seawater Desalination and Waste Water Purification to Produce Drinkable Water. *Desalination* **2019**, *456*, 85−96.

(5) Xu, N.; Hu, X.; Xu, W.; Li, X.; Zhou, L.; Zhu, S.; Zhu, J. Mushrooms as Efficient Solar Steam-Generation Devices. *Adv. Mater.* **2017**, *29*, 1606762.

(6) Finnerty, C. T. K.; Menon, A. K.; Conway, K. M.; Lee, D.; Nelson, M.; Urban, J. J.; Sedlak, D.; Mi, B. Interfacial Solar Evaporation by a 3D Graphene Oxide Stalk for Highly Concentrated Brine Treatment. *Environ. Sci. Technol.* **2021**, *55*, 15435−15445.

(7) Ni, G.; Zandavi, S.; Javid, S.; Boriskina, S. V.; Cooper, T. A.; Chen, G. A Salt-Rejecting Floating Solar Still for Low-Cost Desalination. *Energy Environ. Sci.* **2018**, *11*, 1510−1519.

(8) Zhou, X.; Guo, Y.; Zhao, F.; Yu, G. Hydrogels as an Emerging Material Platform for Solar Water Purification. *Acc. Chem. Res.* **2019**, *52*, 3244−3253.

(9) Zhang, J.; Wang, C.; Shi, J.; Wei, D.; Zhao, H.; Ma, C. Solar Selective Absorber for Emerging Sustainable Applications. *Adv. Energy Sustain. Res.* **2022**, *3*, 2100195.

(10) Chen, C.; Wang, M.; Chen, X.; Chen, X.; Fu, Q.; Deng, H. Recent Progress in Solar Photothermal Steam Technology for Water Purification and Energy Utilization. *Chem. Eng. J.* **2022**, *448*, 137603.

(11) Wu, X.; Chen, G. Y.; Owens, G.; Chu, D.; Xu, H. Photothermal Materials: A Key Platform Enabling Highly Efficient Water Evaporation Driven by Solar Energy. *Mater. Today Energy* **2019**, *12*, 277−296.

(12) Gao, M.; Zhu, L.; Peh, C.; Ho, G. Solar Absorber Material and System Designs for Photothermal Water Vaporization towards Clean Water and Energy Production. *Energy Environ. Sci.* **2019**, *12*, 841−864.

(13) Dao, V.-D.; Choi, H.-S. Carbon-Based Sunlight Absorbers in Solar-Driven Steam Generation Devices. *Global Challenges* **2018**, *2*, 1700094.

(14) Zhang, L.; Bai, B.; Hu, N.; Wang, H. Low-Cost and Facile Fabrication of a Candle Soot/Adsorbent Cotton 3D-Interfacial Solar Steam Generation for Effective Water Evaporation. *Sol. Energy Mater. Sol. Cells* **2021**, *221*, 110876.

(15) Saleque, A. M.; Ma, S.; Ahmed, S.; Hossain, M. I.; Qarony, W.; Tsang, Y. H. Solar Driven Interfacial Steam Generation Derived from Biodegradable Luffa Sponge. *Adv. Sustain. Syst.* **2021**, *5*, 2000291.

(16) Wilson, H. M.; Rahman AR, ARS.; Garg, T.; Jha, N. Recycling of Hazardous Diesel Soot Particles into a High Performance Solar Evaporation Device. *Appl. Surf. Sci.* **2019**, *487*, 951−961.

(17) Sahu, V.; Mishra, M.; Gupta, G.; Singh, G.; Sharma, R. K. Turning Hazardous Diesel Soot into High Performance Carbon/ MnO2 Supercapacitive Energy Storage Material. *ACS Sustainable Chem. Eng.* **2017**, *5*, 450−459.

(18) Sydbom, A.; Blomberg, A.; Parnia, S.; Stenfors, N.; Sandström, T.; Dahlén, S.-E. Health Effects of Diesel Exhaust Emissions. *Eur. Respir. J.* **2001**, *17*, 733−746.

(19) Seaton, A.; Godden, D.; MacNee, W.; Donaldson, K. Particulate Air Pollution and Acute Health Effects. *Lancet* **1995**, *345*, 176−178.

(20) Ramanathan, V. Global Dimming by Air Pollution and Global Warming by Greenhouse Gases: Global and Regional Perspectives. In *Nucleation and Atmospheric Aerosols*; O'Dowd, C. D., Wagner, P. E., Eds.; Springer Netherlands: Dordrecht, 2007, pp 473−483. DOI: 10.1007/978-1-4020-6475-3_94.

(21) Subramanian, R.; Winijkul, E.; Bond, T. C.; Thiansathit, W.; Oanh, N. T. K.; Paw-armart, I.; Duleep, K. G. Climate-Relevant Properties of Diesel Particulate Emissions: Results from a Piggyback Study in Bangkok, Thailand. *Environ. Sci. Technol.* **2009**, *43*, 4213−4218.

(22) Zhang, L.; Li, X.; Zhong, Y.; Leroy, A.; Xu, Z.; Zhao, L.; Wang, E. N. Highly Efficient and Salt Rejecting Solar Evaporation via a Wick-Free Confined Water Layer. *Nat. Commun.* **2022**, *13*, 849.

(23) Li, K.; Chang, T.-H.; Li, Z.; Yang, H.; Fu, F.; Li, T.; Ho, J. S.; Chen, P.-Y. Biomimetic MXene Textures with Enhanced Light-to-Heat Conversion for Solar Steam Generation and Wearable Thermal Management. *Adv. Energy Mater.* **2019**, *9*, 1901687.

(24) Zhao, H.-Y.; Huang, J.; Zhou, J.; Chen, L.-F.; Wang, C.; Bai, Y.; Zhou, J.; Deng, Y.; Dong, W.-X.; Li, Y.-S.; Yu, S.-H. Biomimetic Design of Macroporous 3D Truss Materials for Efficient Interfacial Solar Steam Generation. *ACS Nano* **2022**, *16*, 3554−3562.

(25) Hong, S.; Shi, Y.; Li, R.; Zhang, C.; Jin, Y.; Wang, P. Nature-Inspired, 3D Origami Solar Steam Generator toward Near Full Utilization of Solar Energy. *ACS Appl. Mater. Interfaces* **2018**, *10*, 28517−28524.

(26) Li, X.; Xu, W.; Tang, M.; Zhou, L.; Zhu, B.; Zhu, S.; Zhu, J. Graphene Oxide-Based Efficient and Scalable Solar Desalination under One Sun with a Confined 2D Water Path. *Proc. Natl. Acad. Sci. U.S.A.* **2016**, *113*, 13953−13958.

(27) Fang, Q.; Li, T.; Lin, H.; Jiang, R.; Liu, F. Highly Efficient Solar Steam Generation from Activated Carbon Fiber Cloth with Matching Water Supply and Durable Fouling Resistance. *ACS Appl. Energy Mater.* **2019**, *2*, 4354−4361.

(28) Wang, Y.; Wu, X.; Wu, P.; Zhao, J.; Yang, X.; Owens, G.; Xu, H. Enhancing Solar Steam Generation Using a Highly Thermally Conductive Evaporator Support. *Sci. Bull.* **2021**, *66*, 2479−2488.

(29) Wu, X.; Wu, Z.; Wang, Y.; Gao, T.; Li, Q.; Xu, H. All-Cold Evaporation under One Sun with Zero Energy Loss by Using a Heatsink Inspired Solar Evaporator. *Adv. Sci.* **2021**, *8*, 2002501.

(30) Wang, Y.; Wu, X.; Yang, X.; Owens, G.; Xu, H. Reversing Heat Conduction Loss: Extracting Energy from Bulk Water to Enhance Solar Steam Generation. *Nano Energy* **2020**, *78*, 105269.

(31) Li, J.; Yan, L.; Li, X.; Song, W.; Li, Y. Porous Polyvinyl Alcohol/ Biochar Hydrogel Induced High Yield Solar Steam Generation and Sustainable Desalination. *J. Chem. Environ. Eng.* **2022**, *10*, 107690.

(32) Li, F.; Cai, X.; Jing, G.; Huang, R.; Song, G.; Wang, D.; Chen, W. Facile synthesis of hierarchical SnSe nanosheets-hydrogel evaporators for sustainable solar-powered desalination. *J. Mater. Chem. A* **2022**, *10*, 10672−10681.

(33) Guo, Y.; Zhou, X.; Zhao, F.; Bae, J.; Rosenberger, B.; Yu, G. Synergistic Energy Nanoconfinement and Water Activation in Hydrogels for Efficient Solar Water Desalination. *ACS Nano* **2019**, *13*, 7913−7919.

(34) Zhou, X.; Zhao, F.; Guo, Y.; Zhang, Y.; Yu, G. A Hydrogel-Based Antifouling Solar Evaporator for Highly Efficient Water Desalination. *Energy Environ. Sci.* **2018**, *11*, 1985−1992.

(35) Ahmed, E. M. Hydrogel: Preparation, Characterization, and Applications: A Review. *J. Adv. Res.* **2015**, *6*, 105−121.

(36) Zhao, F.; Bae, J.; Zhou, X.; Guo, Y.; Yu, G. Nanostructured Functional Hydrogels as an Emerging Platform for Advanced Energy Technologies. *Adv. Mater.* **2018**, *30*, 1801796.

(37) Tan, M.; Wang, J.; Song, W.; Fang, J.; Zhang, X. Self-Floating Hybrid Hydrogels Assembled with Conducting Polymer Hollow Spheres and Silica Aerogel Microparticles for Solar Steam Generation. *J. Mater. Chem. A* **2019**, *7*, 1244−1251.

(38) Ricciardi, R.; Auriemma, F.; De Rosa, C. Structure and Properties of Poly(Vinyl Alcohol) Hydrogels Obtained by Freeze/ Thaw Techniques. *Macromol. Symp.* **2005**, *222*, 49−64.

(39) Ricciardi, R.; Auriemma, F.; Gaillet, C.; De Rosa, C.; Lauprêtre, F. Investigation of the Crystallinity of Freeze/Thaw Poly(Vinyl Alcohol) Hydrogels by Different Techniques. *Macromolecules* **2004**, *37*, 9510−9516.

(40) Zhao, L.; Wang, P.; Tian, J.; Wang, J.; Li, L.; Xu, L.; Wang, Y.; Fei, X.; Li, Y. A Novel Composite Hydrogel for Solar Evaporation Enhancement at Air-Water Interface. *Sci. Total Environ.* **2019**, *668*, 153−160.

(41) Sekine, Y.; Ikeda-Fukazawa, T. Structural Changes of Water in a Hydrogel during Dehydration. *J. Chem. Phys.* **2009**, *130*, 034501.

(42) Patel, M.; Azanza Ricardo, C. L.; Scardi, P.; Aswath, P. B. Morphology, structure and chemistry of extracted diesel soot-Part I: Transmission electron microscopy, Raman spectroscopy, X-ray photoelectron spectroscopy and synchrotron X-ray diffraction study. *Tribol. Int.* **2012**, *52*, 29−39.

(43) Li, C.; Fan, L.; Zhu, R.; Li, X.; Wen, P.; Zhao, X.; Wang, G.; Zou, J.; Kim, F. Adjusting Channel Size within PVA-Based Hydrogels via Ice Templating for Enhanced Solar Steam Generation. *ACS Appl. Energy Mater.* **2020**, *3*, 9216−9225.

(44) Kam, C. S.; Leung, T. L.; Liu, F.; Djurišić, A. B.; Xie, M. H.; Chan, W.-K.; Zhou, Y.; Shih, K. Lead removal from water - dependence on the form of carbon and surface functionalization. *RSC Adv.* **2018**, *8*, 18355−18362.

(45) Wu, F.; Li, J.; Tian, Y.; Su, Y.; Wang, J.; Yang, W.; Li, N.; Chen, S.; Bao, L. 3D Coral-like Nitrogen-Sulfur Co-Doped Carbon-Sulfur Composite for High Performance Lithium-Sulfur Batteries. *Sci. Rep.* **2015**, *5*, 13340.

(46) Sitko, R.; Janik, P.; Feist, B.; Talik, E.; Gagor, A. Suspended Aminosilanized Graphene Oxide Nanosheets for Selective Preconcentration of Lead Ions and Ultrasensitive Determination by Electrothermal Atomic Absorption Spectrometry. *ACS Appl. Mater. Interfaces* **2014**, *6*, 20144−20153.

(47) Shaabani, A.; Afshari, R.; Hooshmand, S. E.; Tabatabaei, A. T.; Hajishaabanha, F. Copper Supported on MWCNT-Guanidine Acetic Acid@Fe3O4: Synthesis, Characterization and Application as a Novel Multi-Task Nanocatalyst for Preparation of Triazoles and Bis-(Indolyl)Methanes in Water. *RSC Adv.* **2016**, *6*, 18113−18125.

(48) Kanakaraj, R.; Sudakar, C. Candle Soot Carbon Nanoparticles as High-Performance Universal Anode for M-Ion (M = Li+, Na+ and K+) Batteries. *J. Power Sources* **2020**, *458*, 228064.

(49) Zhang, X.; Schneider, R.; Müller, E.; Mee, M.; Meier, S.; Gumbsch, P.; Gerthsen, D. Electron Microscopic Evidence for a Tribologically Induced Phase Transformation as the Origin of Wear in Diamond. *J. Appl. Phys.* **2014**, *115*, 063508.

(50) Sun, X.; Luo, C.; Luo, F. Preparation and Properties of Self-Healable and Conductive PVA-Agar Hydrogel with Ultra-High Mechanical Strength. *Eur. Polym. J.* **2020**, *124*, 109465.

(51) Wilson, H. M.; Lim, H. W.; Lee, S. J. Highly Efficient and Salt-Rejecting Poly(Vinyl Alcohol) Hydrogels with Excellent Mechanical

Strength for Solar Desalination. *ACS Appl. Mater. Interfaces* **2022**, *14*, 47800−47809.

(52) Zeng, J.; Wang, Q.; Shi, Y.; Liu, P.; Chen, R. Osmotic Pumping and Salt Rejection by Polyelectrolyte Hydrogel for Continuous Solar Desalination. *Adv. Energy Mater.* **2019**, *9*, 1900552.

(53) Higgins, M. W.; Shakeel Rahmaan, A.; Devarapalli, R. R.; Shelke, M. V.; Jha, N. Carbon Fabric Based Solar Steam Generation for Waste Water Treatment. *Sol. Energy* **2018**, *159*, 800−810.